Length-Invariant Cable Actuation of Generalized Miura Origami Tubes as Deployable Cantilevers

Brandon Wong

March 10, 2026

Abstract

The standard straight Miura tube is a widely studied origami pattern known for its single degree-of-freedom rigid folding motion. By generalizing this geometry to model non-parallel longitudinal creases, the resulting "angled" Miura tubes form tapered deployable cantilevers that are uniquely suited for robotic accessories, such as extendible rover wheel hubs or articulated booms. This paper presents an analytical framework to achieve length-invariant cable actuation through these complex geometric structures, enabling multi-cell deployment using a single motor. We derive kinematic equations modeling the tube as intersecting cones. Furthermore, we outline two optimization strategies—longitudinal and latitudinal routing—to minimize cable strain during deployment. While the computational models demonstrate that total cable length strain can be constrained to under 1%, experimental evaluation of a 7-cell prototype reveals significant practical challenges. Notably, the system exhibits low mechanical advantage during initial deployment. Additionally, a friction scaling factor of approximately 1.3× per pulley creates an exponential increase in tension that can cause lightweight hinges to fail under shear loads.

1 Introduction

Miura tubes are a well-studied origami pattern for deployable structures. The standard straight Miura tube is known to have one degree of freedom rigid folding motion, and can be easily modified with thickness offset for thick folding. A single cell of the miura tube consists of 4 parallelograms that can be stacked on top of each other indefinitely in a zig zag pattern. Furthermore, multiple straight tubes can be zippered together to form a stiff and 3D space-filling tesellated metamaterial [1]. Finally, it has been shown that internal cable tensegrities can be used for stiffness or actuation [2].

1.1 Angled tube variant

In this work, we will generalize the geometry and kinematics of the standard straight Miura tube to a variant where the longitudinal creases are not parallel, but at a constant angle. Although angled Miura tubes cannot zipper into a space-filling metamaterial like their straight counterparts, the tapered geometry forms what is essentially a deployable cantilever that is wide at the base for stability while narrow at the end for dexterity. It is likely possible to mechanically program an arbitrary end-effector trajectory into the geometry of the tube. This generalized structure can be used as an "accessory" component to a structure of standard Miura tubes, for example as part of a wheel module for a deployable rover, or as an articulated boom.

1.2 Cable actuation

In [2], Ochalek and Arya present an actuation mechanism for straight Miura tubes utilizing a cable routing that is approximately length-invariant over the course of the tube's actuation, analagous to a

bicycle chain. This allows the structure to be deployed and stowed with a single motor. Additionally, this theoretically allows multiple Miura tube units to be actuated in series, with no overall change to the length of cable needed to be winched.

We now seek to derive an analytical solution for the optimal cable routing through an arbitrary Miura tube geometry, including angled tubes. Section 2 presents definitions and background kinematics. Section 3 presents an intuitive solution, while Section 4 presents an alternate solution that is analytically more complicated but comes with practical advantages. Finally, Section 5 details the experimental realization of this generalized cable mechanism.

2 Angled Miura tube kinematics

In his 2015 ASME paper, Tomohiro Tachi produces a kinematic formulation for single degree of freedom "horns" composed of rigid foldable degree-4 vertices [3]. While Tachi's formulation is complete, an alternate formulation is presented below for the sake of sections 3 and 4.

Let's define the Miura tube to have three states: undeployed where the model is completely folded with cells laying flat over each other, deployed where the model is entirely 3d, and extended where the model is once again fully flat but with no overlap between cells. We assume the model folds rigidly between the three states.

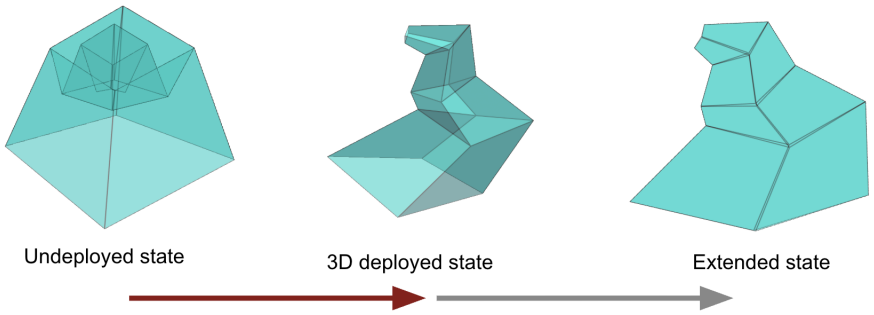


Figure 1: The three kinematic states of a Miura tube.

The creases of the Miura tube can be classified into two categories. Define **latitudinal creases** to the be rings of alternating mountain/valley creases that run roughly perpendicular to the longitudinal creases. **longitudinal creases** to be the long ridges of mountain creases that run along the axis of the tube. The longitudinal creases can then be further classified as the **major ridge**, which is folded in the undeployed state and unfolded in the extended state, and the **minor ridge** which is unfolded in the undeployed state and folded in the extended state.

To ensure a mathematically tractable model, we assume the tube maintains a rhombic cross-section at every point along its axis, characterized by a constant angle ρ between adjacent longitudinal creases. This assumption allows the tube's geometry to be defined by a single crease pattern in the extended state, consisting of two symmetric halves joined along the minor ridges. Rigid foldability is guaranteed by imposing strict flat-foldability constraints: Kawasaki's theorem is applied to all vertices on the major ridge, and the latitudinal creases are required to act as angle bisectors at the minor ridge vertices. Consequently, the entire structure is uniquely defined by the geometry of the major ridge polyline, the tube angle ρ, and the width parameter R_0, as illustrated in Figure 4.

With these parameters, the geometry of the tube can be computed for any intermediate state along the trajectory of the tube's deployment. Each segment of the tube is defined by a cone (technically, pyramid) with an axis and focal point. All segment axes are coplanar. Once the location of the axes and focal points are computed, it is simply a matter of raycasting along the major and minor ridges from each focal point, and placing vertices along the intersection points. Note that two rays in 3d space generally

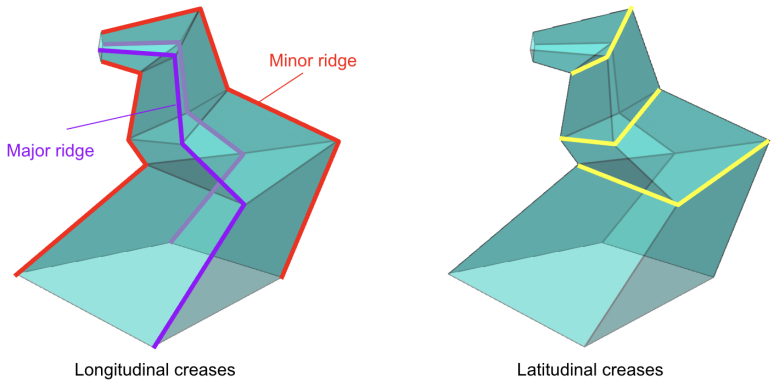


Figure 2: Classification of the types of creases in the Miura tube. This particular tube has 4 cells.

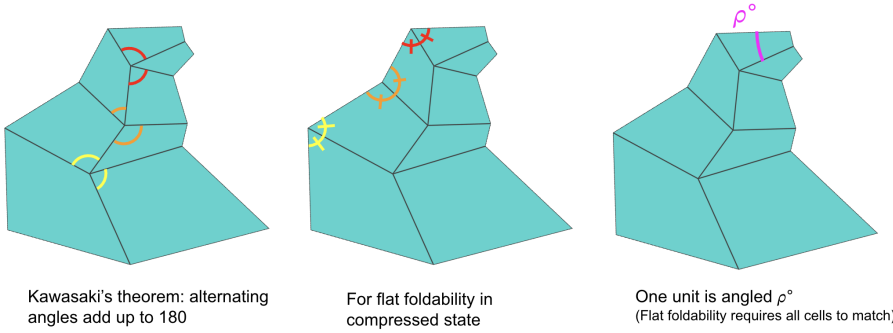


Figure 3: Flat foldability constraints imposed on the crease pattern of the tube's extended state.

do not intersect, unless the computation for the location of the axes and focal points are correct. The details of this computation are described in Appendix A.

The angled miura tube is a natural generalization of the straight miura tube. We can create a single tube that curves in space in a more complex path, such as the tube trajectory shown in Figure 6. The fact that the tube is angled means it can maker sharper bends near the tip, while keeping a wide and sturdy base for support.

3 Longitudinal cable endpoints

In the first formulation to solve the length-invariant cable routing problem, we will optimize all cells of the tube indepently. Assume that each cell has two cables, and assume that the cable endpoints (that is, the pulleys) are located along the cell's longitudinal creases. The cable connecting the major ridges will contract during deployment, while the cable connecting the minor ridges will lengthen during deployment. Our objective is to place the endpoints of the two cables in such a way that the sum of the two cable lengths remain as constant as possible during actuation from the undeployed state to the 3d deployed state.

3.1 Geometry

Define the geometry of an angled Miua cell with the following parameters, illustrated in Figure 7:

- ρ: angle between adjacent fold lines
- a_1, b_1: the arc length across a facet at the radius of the start and end points of cable 1, respectively.

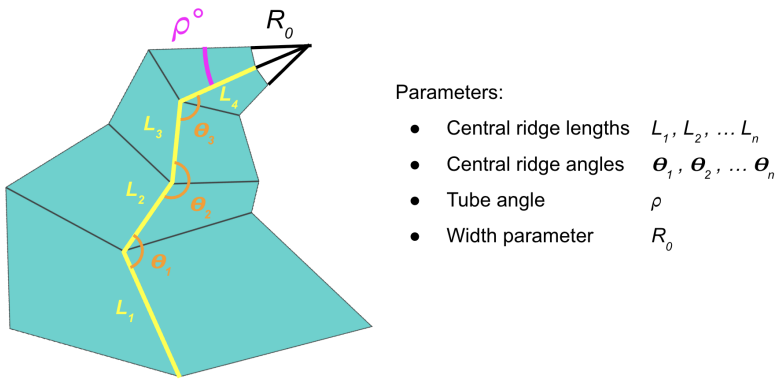


Figure 4: Minimal parametrization to fully define the geometry of the angled Miura tube.

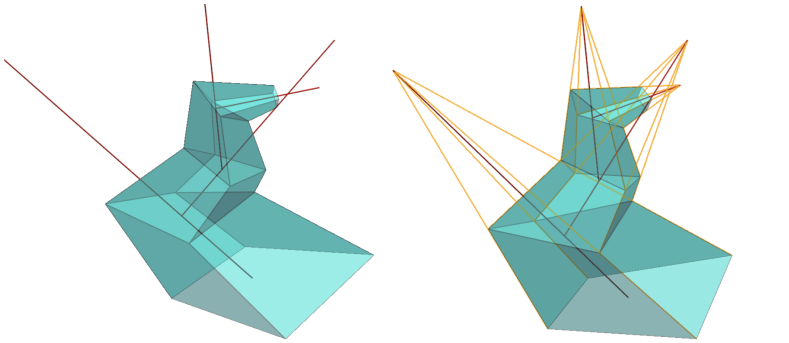


Figure 5: The 3d geometry of an angled Miura tube can be modeled as a series of intersecting cones.

This is such that $\frac{a_1}{\rho}$ and $\frac{b_1}{\rho}$ are the straight-line distances from the tube center to the cable start and end points, respectively.

- L_1, L_2: the lengths of cables 1 and 2
- l_1, l_2: the angle between the two minor ridges, and the angle between the two major ridges
- γ, ϕ: the fold angles of the major and minor ridge creases, respectively.

The resulting optimization problem has 4 parameters (a_1, b_1, a_2, b_2) bounded by the tube geometry (ie, the length of each longitudinal crease), while γ will serve as the structure's primary deployment parameter.

For the following analysis, we will first derive both an exact model of how the cable lengths change over the course of deployment as well as approximate model for small ρ. First, we can relate γ and ϕ as corners on a spherical square with the following relation:

$$\phi(\gamma) = 2\arctan\left(\frac{1}{\tan\left(\frac{\gamma}{2}\right)\cos\rho}\right) \approx \pi - \gamma \tag{1}$$

Next, we can relate l_1 and l_2 to the actuating fold angles γ and ϕ using the spherical law of cosines:

$$\cos l_1(\gamma) = \cos^2\rho + \sin^2\rho\cos\gamma \approx 1 - \rho^2 + \rho^2\cos\gamma \tag{2}$$

$$\cos l_2(\gamma) = \cos^2\rho + \sin^2\rho\cos\phi \approx 1 - \rho^2 + \rho^2\cos\phi(\gamma) \tag{3}$$

Then, we can relate the cable lengths L_1 and L_2 to the diagonal angles l_1 and l_2 using the Euclidean law of cosines:

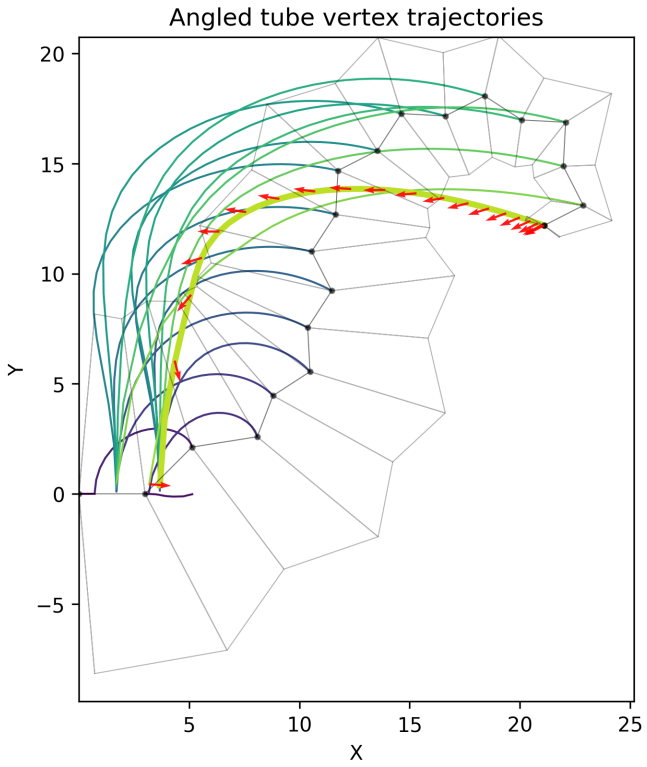


Figure 6: A trajectory of a complex Miura tube projected to the xy plane. This tube uses an angle of $\rho = 10°$. The red arrows indicate the position and orientation of the end-effector throughout the trajectory.

$$L_1(\gamma) = \frac{1}{\rho}\sqrt{a_1^2 + b_1^2 - 2a_1 b_1 \cos l_1(\gamma)} \tag{4}$$

$$L_2(\gamma) = \frac{1}{\rho}\sqrt{a_2^2 + b_2^2 - 2a_2 b_2 \cos l_2(\gamma)} \tag{5}$$

Although the total cable length will never be exactly constant, we can approximate length conservation by constraining the starting length to equal the final length, i.e. $L_{1,start}+L_{2,start} = L_{1,end}+L_{2,end}$. Assume that the tube starts in the flat undeployed state with $\gamma = 0$ and ends in the 3d deployed stae with $\gamma = \frac{\pi}{2}$. Combining the above equations, we get the exact governing equation:

$$\begin{aligned}&\sqrt{a_2^2 + b_2^2 - 2a_2 b_2 \cos^2(\rho) + \frac{2a_2 b_2 \sin^4(\rho)}{\sin^2(\rho) - 2}} \quad + \sqrt{a_1^2 - 2a_1 b_1 \cos^2(\rho) + b_1^2} \\ &= \sqrt{a_2^2 - 2a_2 b_2 \cos(2\rho) + b_2^2} + |a_1 - b_1|\end{aligned} \tag{6}$$

or for small ρ, we can approximate with:

$$\begin{aligned}&\sqrt{{a_1}^2 - 2\,a_1\,b_1 + {b_1}^2} + \sqrt{{a_2}^2 + {b_2}^2 + 2\,a_2\,b_2\,(2\,\rho^2 - 1)} \\ &= \sqrt{{a_1}^2 + {b_1}^2 + 2\,a_1\,b_1\,(\rho^2 - 1)} + \sqrt{{a_2}^2 + {b_2}^2 + 2\,a_2\,b_2\,(\rho^2 - 1)}\end{aligned} \tag{7}$$

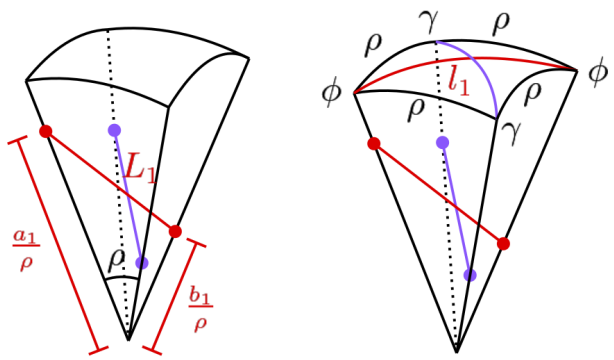
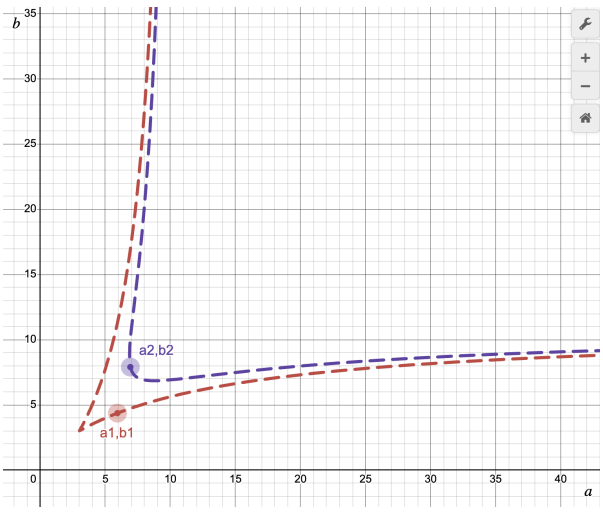


Figure 7: Parametrization of the two cables in a single angled Miura tube cell in the longitudinal formulation.

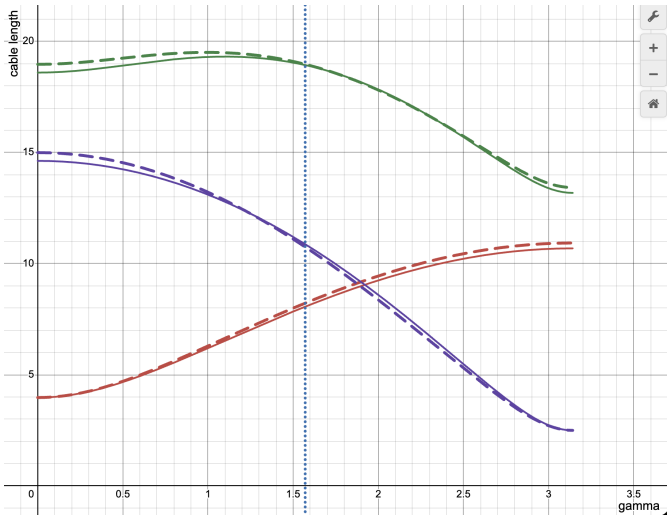
3.2 Solution space

It is not obvious to see whether or not a solution to equation (6) exists. Although there are 4 variables to optimize, the parameters are decoupled between the two cables. In Figure 8a, we hold a_2, b_2 constant and plot a_1 vs b_1 (red) and the same for the other cable (purple). In practice, there will be geometric bounds on each parameter (ex: $a_1 \in [2, 4]$). But as long as the isocurves for each pair of cable parameters intersect their respective bounded design spaces, a solution exists for a length invariant cable routing within this cell of the tube.

An example of the cable lengths over the course of deployment for a solution to the governing equation is shown in Figure 8b. The minor cable (red) lengthens monotonically while the major cable (purple) contracts monotonically. As a result, the total cable lengths (green) is not constant but remains within 3% strain during deployment from $\gamma = 0$ to $\gamma = \frac{\pi}{2}$. However, it is worth noting in Figure 8b that the derivatives $\partial L_1/\partial\gamma$ and $\partial L_2/\partial\gamma$ are close to zero for $\gamma \approx 0$. This means the mechanism has little mechanical advantage at the start of the deployment.



(a) A projection of the 4 dimensional solution space. The governing equation is satisfied while both parameters lie on their respective isocurves.



(b) Example solution to the governing equation. Red is a plot of $L_1(\gamma)$, purple is a plot of $L_2(\gamma)$, and green is the total $L_{total}(\gamma)$. Solid lines are exact values, while dashed lines approximate with small ρ.

Figure 8: Solution space for the longitudinal cable routing problem.

4 Latitudinal cable endpoints

In this formulation, we place cable endpoints along the latitudinal creases instead of the longitudinal creases

4.1 Geometry

The position of a pulley is defined by the geometry of the latitudinal crease it lies on, and a fractional interpolation parameter ξ that defines how far along the crease the pulley is. A latitudinal crease has one vertex $\mathbf{P}_{\text{major}}$ on the major ridge and one vertex $\mathbf{P}_{\text{minor}}$ on the minor ridge. The length of this crease is constant, but the two vertices move in 3D space as a function of the deployment parameter γ. Define ξ such that $\xi = 1$ will place the pulley coincident with the minor ridge, and $\xi = 0$ will place it coincident with the major ridge. Therefore, the position of a pulley is given by the linear interpolation:

$$\mathbf{p}(\gamma) = (1 - \xi)\mathbf{P}_{\text{major}}(\gamma) + \xi\mathbf{P}_{\text{minor}}(\gamma) \tag{8}$$

To actuate n cells of the tube, we will need $2n+2$ pulleys for $2n$ cables. Without loss of generalization, we can compute the length of a single cable segment spanning the i-th and $(i+1)$-th pulley as the Euclidean distance of its two endpoints:

$$L_i(\gamma) = \|\mathbf{p}_{i+1}(\gamma) - \mathbf{p}_i(\gamma)\| \tag{9}$$

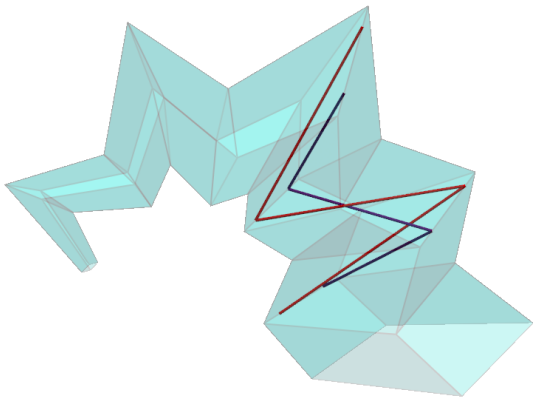
The cable routing is composed of two sub-routings: one that lengthens during actuation, and one that contracts. To prevent segments of cable that are "inactive" (ie, do not change in length during actuation), we assume that subsequent cable segments within a sub-routing share pulleys. Therefore, the length $L_{total,1}$ of a sub-routing can be fully defined by the continuous vector of interpolation parameters $\Xi_1 = [\xi_1, \xi_2, \ldots, \xi_{n+1}]$ to place each pulley on its crease, and the discrete choice of $n + 1$ latitudinal creases that each pulley lies on. While the optimization framework permits the selection of any arbitrary set of latitudinal creases, practical implementation favors the use of alternating mountain folds located near the structural base. This placement maximizes the change in individual cable lengths, leaing to improved mechanical advantage. Additionally, for the sake of simplicity of assembly, assume that the two sub-routings use the same set of creases, but with different interpolation parameters. Therefore, the total optimization problem is reduced to a concatenated vector of interpolation parameters $\Xi = [\xi_1, \xi_2, \ldots, \xi_{n+1}, \xi_{n+2}, \ldots, \xi_{n+2}] \in [0, 1]^{2n+2}$ for the two sub-routings.

4.2 Optimization

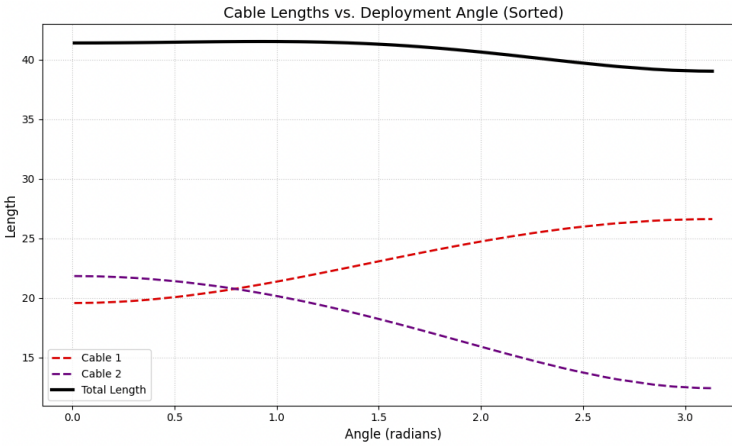
Unlike the longitudinal formulation, the latitudinal approach requires a global optimization. Our objective function $\mathcal{J}(\Xi)$ seeks to minimize the change in total cable length during deployment, while maximizing the magnitude of length change of each sub-routing for mechanical advantage. This can be expressed as the following ratio:

$$\mathcal{J}(\Xi) = \frac{\max L_{total} - \min L_{total}}{|L_{total,1}(\gamma_{end}) - L_{total,1}(\gamma_{start})| + |L_{total,2}(\gamma_{end}) - L_{total,2}(\gamma_{start})|} \tag{10}$$

The objective function is evaluated numerically by sweeping the deployment parameter γ. The optimization could be solved using standard constrained optimizization solvers, but in practice the performance varies only slightly within a certain parameter space, and other factors such as fabrication convenience can be considered. For example, a near optimal routing with $\Xi = [0.2, 0.2, 0.2, 0.2, 0.8, 0.8, 0.8, 0.8]$ is shown below in Figure 9a. In this configuration, the total cable length strains by less than 0.7%, while each of the two cables strain by almost 10%.



(a) A render of a deployed tube with $n = 3$ cells actuated by connecting cables across alternating latitudinal mountain folds. The cables are connected to a single winch at the bottom, and fixed to the structure at the top.



(b) The change in cable lengths over the deployment trajectory. The total cable length is nearly constant for $\gamma \in [0, \frac{\pi}{2}]$.

Figure 9: An example of a latitudinal cable routing in an angled Miura tube.

5 Prototype and experimental results

Utilizing latitudinal crease-aligned pulleys provides distinct advantages over the longitudinal alternative, primarily because this configuration minimizes off-axis cable skew and eliminates inactive cable lengths. Furthermore latitudinal mountain folds inherently offer more clearance for mounting a hinge pin and pulley assembly while accomodating thick panel folding. However, the overall experimental performance of this initial prototype was limited. As anticipated by the kinematic model, the low mechanical advantage at the onset of deployment required excessive force to initiate movement. Consequently, the tube could only be reliably actuated within a narrow operational envelope near the fully 3D deployed state ($\gamma \approx \frac{\pi}{2}$) where mechanical advantage is maximized. Outside this optimal range, applying the required cable tension resulted in structural failure, causing the non-hinge pulleys to tear away from the assembly.

5.1 Pulley hinge assembly

Refer to the closeup in Figure 10. The hinge consists of a 4 inch bolt as the pin with 3d printed knuckles bolted to the two facets. Each pulley consists of a nylon bushing and washer also assembled around the hinge pin. The cable is wrapped around the bushing, with the washer serving as a retainer to prevent the cable from slipping off. This pulley is cheap and simple, and performs decently for its size and price, but the friction scaling is still significant.

5.2 Failure of non-pulley hinges

To maximize compact foldability, the non-pulley hinges in this prototype were constructed using tape. Although these tape joints exhibit adequate strength in the transverse direction, they are highly susceptible to failure when subjected to significant shear loads. During testing, the cumulative friction within the pulley system increased the required cable tension to a level that induced shear failure at these tape joints. Future iterations of this prototype will require more robust hinge designs, which will likely necessitate a compromise on the structure's compact foldability.



Figure 10: A prototype of an a 7-celled angled Miura tube actuated by 8 latitudinal pulleys. Left: overall view, right: closeup of the concentric hinge-pulley assembly.

5.3 Cable tensioning

Though the total cable length is near-constant, the actuation mechanism must accomodate a small amount of strain. Initially, two springs were placed in series with the cable to manage this strain; however, friction within the pulleys isolated the tension, preventing the springs from effectively taking up slack located in other segments of the routing. An ideal solution would employ an elastic bungee-style cable possessing a uniform stiffness and the capacity for reasonable strain without yielding. This would allow slack to be distributed evenly across the system. Ultimately, cable tensioning presents an optimization tradeoff: increasing tension exacerbates system friction, whereas insufficient tension results in detrimental cable slack.

5.4 Pulley skew

The physical pulley axes in the prototype are constrained to align with the lateral fold axes of the origami structure. In practice, however, the wrapping angle of the cable rarely aligns perfectly with these prescribed axes. Though the latitudinal pulley framework improves on this aspect compared to the longitudinal framework, this skew is still non-negligible. This misalignment introduces additional friction into the system and, under severe skew, can cause the cable to slip off the pulley entirely, an issue that must be addressed in subsequent prototype designs. Future designs might consider the use of spherical bearings or compound pulleys.

5.5 Pulley friction

By far the biggest limiting factor in the practical realization of the cable mechanism is the exponential growth of tension along the cable due to pulley friction in series. In the prototype described above, the nylon bushings around the hinge pin was a fairly effective pulley bearing for its size and price, but the friction scaling even in the idealized setup shown in Figure 11 is still around 1.3× per pulley, which scales

up to at least an 8× increase in tension for the 8 pulley setup of this prototype. When off-axis skew and variable wrapping angles are introduced, this friction scaling becomes exponentially worse, making actuation nearly impossible without a beefy motor and shear-resistant hinges. Future prototypes could use fancier bearings to reduce the friction per pulley, but the fundamental problem of exponential growth remains and it's only a matter of a few more pulleys in the system before tension becomes once again unmanageable.

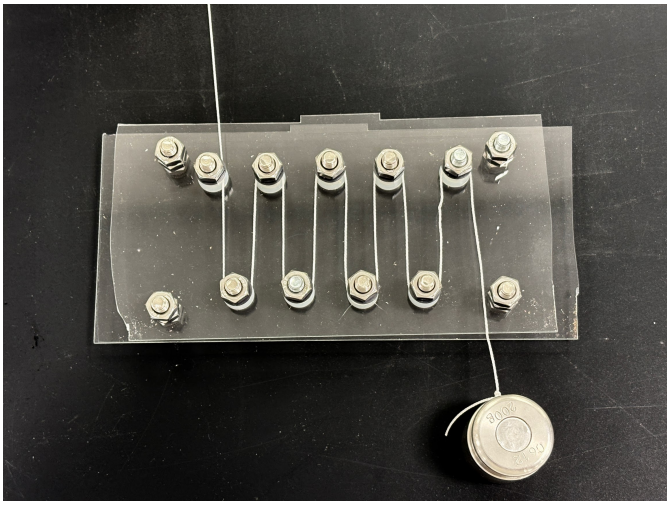


Figure 11: An model of the 8 pulleys used to actuate the latitudinal cable prototype, idealized to maintain a constant wrapping angle and no off-axis skew. By comparing the tension of the output string to the weight loaded on the output cable, we can estimate the friction scaling factor of the pulleys.

5.6 Elastic decay

Because the Miura tube is theoretically a single degree-of-freedom rigid mechanism, actuating a single cell should be mathematically sufficient to deploy the entire structure. In physical implementations, however, compliance leads to elastic decay, necessitating the actuation of multiple cells to achieve reliable deployment. While elastic decay has been investigated in standard straight Miura tubes, these principles have not yet been formalized for the angled variants explored in this work. Consequently, designers face a significant tradeoff: routing more cables reduces elastic decay and ensures a more predictable deployment trajectory, but introduces additional pulleys that compound system friction.

6 Conclusion

This research demonstrates that it is geometrically possible to design a length-invariant cable routing for an angled Miura tube, allowing a multi-celled deployable cantilever to be actuated with a single winch. By modeling the tube's kinematics using intersecting cones, we developed two distinct optimization approaches. The latitudinal routing formulation proved particularly advantageous by minimizing off-axis cable skew and seamlessly integrating with the required hinge offsets for thick folding. However, physical prototyping exposed several operational limitations. The exponential accumulation of friction—measured in idealized conditions at a 1.3× scaling factor per pulley—overwhelmed the structural integrity of the tape-based hinges due to excessive shear loads on the hinges. Furthermore, balancing cable tension to prevent slack without worsening friction remains a critical hurdle, as springs placed in series with the cables are neutralized by localized pulley friction. Future development must address the misalignment of pulley axes relative to cable wrapping, investigate methods to counteract elastic decay without adding

excessive pulleys, and incorporate shear-resistant hinges and high-efficiency bearings to make physical actuation feasible.

References

[1] Evgueni T. Filipov, Tomohiro Tachi, and Glaucio H. Paulino. "Origami tubes assembled into stiff, yet reconfigurable structures and metamaterials". In: *Proceedings of the National Academy of Sciences* 112.40 (2015), pp. 12321–12326. DOI: 10.1073/pnas.1509465112. eprint: https://www.pnas.org/doi/pdf/10.1073/pnas.1509465112. URL: https://www.pnas.org/doi/abs/10.1073/pnas.1509465112.

[2] Megan Ochalek and Manan Arya. "Design and Modeling of Pre-stressed, Flat-Folding, Modular Origami Tube Structures". In: *AIAA SCITECH 2024 Forum*. DOI: 10.2514/6.2024-1043. eprint: https://arc.aiaa.org/doi/pdf/10.2514/6.2024-1043. URL: https://arc.aiaa.org/doi/abs/10.2514/6.2024-1043.

[3] Tomohiro Tachi. "Designing Rigidly Foldable Horns Using Bricard's Octahedron". In: *Journal of Mechanisms and Robotics* 8.3 (Mar. 2016), p. 031008. ISSN: 1942-4302. DOI: 10.1115/1.4031717. eprint: https://asmedigitalcollection.asme.org/mechanismsrobotics/article-pdf/8/3/031008/6254190/jmr_008_03_031008.pdf. URL: https://doi.org/10.1115/1.4031717.

A Forward Kinematic equations

This appendix provides the analytical formulation for the forward kinematics to compute the 3d shape of the Miura tube as a function of deployment angle, as implemented in the computational model. As mentioned in Section 2, the geometry of the tube can be modeled as a series of intersecting cones, where each cone corresponds to a segment of the tube. Each cone is defined by its axis (a line on the XY plane) and its focal point (the center of the cone). The vertices of the tube are then found at the intersection points of rays cast from these focal points along the directions defined by the major and minor ridges.

A.1 Segment Axis Orientations

We define the absolute orientation of each segment's axis in the XY plane as α_i, distinguishing it from the input polyline angles θ_i which represent the relative angles between segments in the flattened extended state.

Given the major fold angle γ (and its corresponding minor fold angle ϕ), the absolute axis angles are computed iteratively. For the first segment, the axis aligns with the initial polyline angle: $\alpha_0 = \theta_0$. For subsequent segments ($i \geq 1$), the relative sector angle β_i between segment $i-1$ and i in the extended state is:

$$\beta_i = \frac{\pi - \theta_i}{2} \tag{11}$$

When the tube deploys, this sector folds. We compute the intermediate fold angle ψ_i across this sector using the spherical square relation:

$$\psi_i = 2 \arctan\left(\frac{1}{\tan\left(\frac{\phi}{2}\right)\cos\beta_i}\right) \tag{12}$$

The 3D angular change $\Delta\alpha_i$ between the axes of segment $i-1$ and segment i is then found via the spherical law of cosines:

$$\Delta\alpha_i = \pi - \arccos\left(\cos^2\beta_i + \sin^2\beta_i \cos\psi_i\right) \tag{13}$$

Finally, the absolute orientation of the i-th axis in the XY plane is updated by applying this angular change in the direction specified by the sign of the original polyline angle:

$$\alpha_i = \alpha_{i-1} + \Delta\alpha_i \cdot \text{sgn}(\theta_i) \tag{14}$$

This gives us a unit direction vector for each segment's axis: $\mathbf{u}_i = (\cos\alpha_i, \sin\alpha_i)$.

A.2 Cone Center Points (Focal Points)

As established in Section 2, each segment of the tube is defined by a cone with an axis and focal point. Furthermore, all segment axes are coplanar and lie entirely within the XY plane.

To locate the cone centers $\mathbf{C}_i$ (focal points) and the intersection points $\mathbf{I}_i$ between adjacent axes, we must account for the longitudinal contraction of the tube during deployment. We define the 3D shrinkage factor s based on the minor ridge angle l_2 (which is given in Equation 2):

$$s = \cos^2\left(\frac{l_2}{2}\right) \tag{15}$$

Let L_i be the length of the i-th segment of the defining polyline (refer to Figure 4, not to be confused with cable length), and R_0 be the initial width parameter defining the distance to the first cone center. We define a sequence of radii W_i representing the geometric offsets for each segment. For the initial segment:

$$W_0 = R_0 \tag{16}$$

For all subsequent segments ($i \geq 1$), the offset is reduced by the cumulative sum of the preceding segment lengths:

$$W_i = R_0 - \sum_{j=0}^{i} L_j \tag{17}$$

With the unit vectors $\mathbf{u}_i$ and the shrinkage factor s computed, the locations of the cone centers $\mathbf{C}_i$ and axis intersections $\mathbf{I}_i$ are defined by a sequence of recurrence equations starting at the origin ($\mathbf{I}_0 = \begin{bmatrix}0 & 0 & 0\end{bmatrix}^\top$):

$$\mathbf{C}_i = \mathbf{I}_i + (W_i \cdot s)\mathbf{u}_i \qquad \text{for } 0 \leq i \leq n-1 \tag{18}$$

$$\mathbf{I}_{i+1} = \mathbf{C}_i - (W_{i+1} \cdot s)\mathbf{u}_i \qquad \text{for } 0 \leq i < n-1 \tag{19}$$

A.3 Vertex Generation via 3D Ray Intersection

The physical geometry of the rigid-folding Miura tube mandates that the creases forming each segment emanate radially from that segment's focal point $\mathbf{C}_i$. Because the vertices of the tube act as spherical linkages, it is mathematically natural to define the 3D position of the longitudinal creases using a local spherical coordinate system centered at each $\mathbf{C}_i$.

In this local system, a direction vector is defined by an azimuth angle (relative to the global X-axis in the XY plane) and an elevation angle (relative to the XY plane). Since the focal points are positioned "outside" the physical tube geometry, the rays pointing toward the tube must point backwards along the segment axis, which is achieved by adding π to the base axis angle α_i.

From this central backward axis, the 4 longitudinal ridges of the tube diverge by exactly half the angle of the respective ridge angles.

- The major ridges (top and bottom) deviate strictly in the elevation direction by $\pm l_2/2$.
- The minor ridges (left and right) deviate strictly in the azimuth direction by $\pm l_1/2$.

Therefore, for any segment i, we can construct four directional rays corresponding to the four ridges:

$$\mathbf{d}_{i,\text{top}} = \text{SphericalDir}(\text{azimuth} = \alpha_i + \pi, \text{elevation} = l_2/2) \tag{20}$$

$$\mathbf{d}_{i,\text{right}} = \text{SphericalDir}(\text{azimuth} = \alpha_i + l_1/2 + \pi, \text{elevation} = 0) \tag{21}$$

$$\mathbf{d}_{i,\text{bottom}} = \text{SphericalDir}(\text{azimuth} = \alpha_i + \pi, \text{elevation} = -l_2/2) \tag{22}$$

$$\mathbf{d}_{i,\text{left}} = \text{SphericalDir}(\text{azimuth} = \alpha_i - l_1/2 + \pi, \text{elevation} = 0) \tag{23}$$

where the conversion to a Cartesian unit vector is given by $\text{SphericalDir}(\theta, \phi) = \begin{bmatrix}\cos\phi\cos\theta & \cos\phi\sin\theta & \sin\phi\end{bmatrix}^\top$.

The intermediate latitudinal creases of the tube are formed at the exact boundary where segment $i-1$ transitions into segment i. Therefore, the 4 vertices $\mathbf{V}_{i,j}$ that define the i-th latitudinal cross-section are mathematically determined by computing the 3D intersection of the j-th ray emanating from $\mathbf{C}_{i-1}$ with the corresponding j-th ray emanating from $\mathbf{C}_i$.

For example, the right-side vertex $\mathbf{V}_{i,\text{right}}$ is the solution to the intersection of two 3D lines:

$$\mathbf{V}_{i,\text{right}} = (\mathbf{C}_{i-1} + t\mathbf{d}_{i-1,\text{right}}) \cap (\mathbf{C}_i + u\mathbf{d}_{i,\text{right}}) \tag{24}$$

Because the input parameters enforce flat-foldability, these paired rays are coplanar and intersect perfectly. This process is repeated for $j \in \{\text{top, right, bottom, left}\}$ across all $n-1$ internal segment transitions to compute the complete 3D vertex mesh of the angled Miura tube.

B IMECE abstract

Title: Length-Invariant Cable Actuation for Generalized Angled Miura Tubes as Deployable Cantilevers

The principles of origami engineering allow for the creation of advanced functional systems characterized by high stowage ratios and programmable shape-morphing capabilities. While standard straight Miura-ori tubes are well-characterized for their single-degree-of-freedom (1-DOF) rigid foldability and potential for zippering into stiff metamaterials, their geometric uniformity limits their application for complex pre-programmed trajectories. This research generalizes the kinematics of the Miura tube into an "angled" variant where longitudinal creases are non-parallel. This transformation enables the creation of tapered, deployable cantilevers that provide a wide, stable base for structural support and a narrow tip for high-dexterity positioning, making them ideal for space-constrained applications such as deployable rover modules or articulated robotic booms.

The primary contribution of this work is the development and implementation of a length-invariant cable routing mechanism, analogous to a bicycle chain, which enables the deployment and stowage of multi-cell structures using a single motor. While the kinematics of rigid-folding origami structures like this are already well studied, this work presents a framework of a series of intersecting cones as an alternative kinematic formulation specific to this angled Miura tube context. We then apply this formulation to drive the novel actuation optimization framework.

For the geometry of this actuation system, we evaluate two distinct optimization strategies: a longitudinal formulation, where pulleys are located along longitudinal creases of the tube, and a latitudinal formulation, which utilizes fractional interpolation along latitudinal creases of the tube. The latitudinal framework is shown to offer superior practical advantages, including improved clearance for embedding pulley assemblies within hinges, the elimination of "inactive" cable segments between cells, and minimized off-axis cable skew.

Computational models demonstrate that total cable length strain can be constrained to under 1%, while individual cables doing mechanical work will strain up to 10%. However, preliminary experimental verification using a 7-cell prototype featuring 3D-printed pulley-hinge assemblies reveals significant practical scalability challenges. Attempts to actuate this prototype indicate that the system exhibits low mechanical advantage during initial deployment states, requiring excessive force to initiate movement. Furthermore, non-negligible pulley friction leads to an exponential increase in cable tension as the complexity of tube designs increase, leading to shear failure if lightweight hinge designs are used.

Ongoing work aims to formalize the elastic decay of the rigid-foldability of these tubes in order to minimize the necessary actuation. Additional work aims to mitigate friction scaling with the use of high-efficiency spherical bearings or more complex pulley assemblies, or explore elastic cable materials to better pick up slack while evenly distributing tension throughout the system. This work concludes that while the analytical models for angled Miura tubes offer a useful theoretical framework for internally actuated programmable trajectories, the practical realization of cable-driven origami deployable structures requires careful mechanical design to manage friction and structural integrity in order to scale the complexity of these structures.